Compact energy–time entanglement source using cascaded nonlinear interactions

Lefebvre, P.; Valivarthi, R.; Zhou, Q.; Oesterling, L.; Oblak, D.; Tittel, W.

DOI
10.1364/JOSAB.404312

Publication date
2021

Document Version
Accepted author manuscript

Published in
Journal of the Optical Society of America B: Optical Physics

Compact energy-time entanglement source using cascaded non-linear interactions

P. LEFEBVRE[1], R. VALIVARTHI[1,2], Q. ZHOU[1,3,6], L. OESTERLING[4], D. OBLAK[1,7] AND W. TITTEL[1,5,8]

[1] *Department of Physics and Astronomy, and Institute for Quantum Science and Technology, University of Calgary, Calgary, T2N 1N4, Canada*
[2] *Division of Physics, Mathematics and Astronomy, California Institute of Technology, Pasadena, California 91125, USA*
[3] *Institute of Fundamental and Frontier Sciences, and the School of Optoelectronic Science and Engineering, University of Electronic Science and Technology of China (UESTC), Chengdu, China*
[4] *Battelle Memorial Institute, 505 King Avenue Columbus, Ohio 43201, USA*
[5] *QuTech, and Kavli Institute of Nanoscience, Delft Technical University, Delft, The Netherlands*
[6] *zhouqiang@uestc.edu.cn*
[7] *doblak@ucalgary.ca*
[8] *W.Tittel@tudelft.nl*

Abstract: Entangled photon pair sources are essential for applications such as quantum communication and metrology. Here we present a compact energy-time entangled photon pair source at telecom wavelengths realized through cascaded second harmonic generation and spontaneous parametric down conversion in a single periodically-poled lithium niobate waveguide. We introduce and characterize methods to diminish the effects of Raman scattering, the principal being quasi-CW pumping. The quality of energy-time entanglement produced by the compact source is analyzed using two-photon interference and Franson interference, and visibilities as high as 93.9% ± 0.4% and 90.5% ± 0.6% are achieved, respectively.

1. Introduction

Quantum entanglement counterintuitively predicts nonclassical correlations among physically separable subsystems, hence the famous appellation "spooky action at a distance" [1,2]. In the last three decades, entanglement has attracted much attention for its abundant uses in the most fundamental tests of quantum mechanics [3] and for the development of applications of quantum information technologies [4–6]. More particularly, devices that produce entangled photons are readily available for multiple applications [7,8]. A popular way to generate quantum entangled photons is based on parametric fluorescence, such as spontaneous parametric down conversion (SPDC) and spontaneous four wave mixing (SFWM) from second-order ($\chi^{(2)}$) and third-order ($\chi^{(3)}$) non-linear materials, respectively [9].

In the second-order SPDC process, a pair of quantum-correlated photons (known as a signal-idler photon pair) may, with some probability, be generated while a pump photon is annihilated. Compared with the $\chi^{(3)}$ SFWM process, it is in general more effective and does not suffer from noise caused by Raman scattering due to the large separation between the pump and the created photons' wavelengths. Of particular interest for efficient SPDC are materials with high effective non-linear coefficients , e.g. lithium niobate and potassium titanyl phosphate [10]. These crystals can be engineered into periodically poled waveguides, ensuring phase matching at desirable wavelengths and good mode overlap of the pump light with the proper regions of the crystal.

Photon pair creation in the telecom band of around 1550 nm can be realized by pumping a single periodically poled lithium niobate (PPLN) waveguide with a pump laser at 1532.7 nm, and taking advantage of cascaded second harmonic generation and spontaneous parametric down

conversion (SHG-SPDC) second-order nonlinear processes. While the photon pair generation stems from the SPDC process, and could be realized directly from a pump photon of energy equal to the sum of the energies of the pair photons, it is convenient to avoid working with photons of multiple wavelengths in integrated devices. The cascaded processes affords a system in which the wavelength of the pump and of the created photon pairs are all in the telecom band (e.g. 2×1532.7 nm $\xrightarrow{SHG}$ 766.4 nm $\xrightarrow{SPDC}$ 1530.3 nm + 1535.0 nm), allowing the use of standard telecommunication components for quantum communications. Inspired by this idea, K. Hirosawa *et. al.* generated squeezed vacuum through cascaded second-order nonlinear processes [11], and M. Hunault *et. al.* and S. Arahira *et. al.* realized the generation of time-bin entanglement and polarization entanglement, respectively [12, 13].

Polarization-entangled photon pairs are simple to generate and detect using common optical components; such sources have been realized numerous times. However, time-bin entanglement is often favored in quantum network applications due to its robustness to perturbations in fibers over long distances. The limiting factors to the rate and quality of time-bin entangled pairs are related to the rate at which the pump pulses are generated and to the bandwidth mismatch between the pump and the generating pairs [14]. The effect of bandwidth mismatch is greatly reduced for energy-time entanglement generation, due to continuous wave pumping, but the dead-times and timing jitter of single photon detectors limit the performance. Recent advances in detection technology, such as the advent of superconducting nanowire single photon detectors (SNSPD) with low jitter and very short dead times [15] can make energy-time entanglement sources competitive, in term of count rates, with time-bin entanglement sources.

In this paper, energy-time entangled photon pairs are generated in a single PPLN waveguide based on cascaded SHG-SPDC processes. The waveguide was fabricated through reverse-proton-exchange, thus avoiding sensitivity to photo-refractive effects [16, 17]. The performance of the photon pair source is characterized by measuring the individual signal and idler photon count rates and the coincidence count rates for different pump powers. Furthermore, we assess the quality of two-photon interference using a single unbalanced fiber Michelson interferometer as well as two interferometers in a Franson-type configuration. Imperfections such as Raman scattering in the fibers as well as methods to overcome them are discussed.

2. Methods

Light from a continuous-wave laser at $\omega_p = 1532.7$ nm is sent through an intensity-modulator to create pulses with a duration of 100 ns at a frequency of 500 kHz, as shown in Figure 1. This light is then fed to an erbium-doped fiber amplifier (EDFA), where it is amplified to an average power of ~ 12 mW, implying a peak power of ~ 240 mW. A polarization controller is used to align the polarization of the pump light to the proper axis of the PPLN waveguide. The light also passes through an attenuator, which controls the amount of pump light input to the waveguide. This light is then sent to a fiber-bonded waveguide, inside of which it undergoes cascaded SHG and SPDC. The light proceeds through multiple dense wavelength division multiplexing filters that separate the pump light at 1532.7 nm from the photon pairs. A further series of filters defines frequency non-degenerate photon pairs of 0.5 nm bandwidth with central wavelengths of idler and signal photons at $\omega_i = 1530.3$ nm and $\omega_s = 1535.0$ nm, respectively. For non-degenerate photon pairs and assuming a monochromatic pump, the resulting state can be described by:

$$\begin{aligned} |\psi\rangle &= \int\int d\omega_s d\omega_i \; \delta(\omega_p - \omega_s - \omega_i) \\ &\quad \times f(\omega_p, \omega_s, \omega_i) \, |\omega_s\rangle \, |\omega_i\rangle \,, \qquad (1) \\ &\equiv \int\int dt dt' \; \delta(t - t') \, |t\rangle_s \, |t'\rangle_i \,, \\ &= \int dt \, |t\rangle_s \, |t\rangle_i \,. \qquad (2) \end{aligned}$$

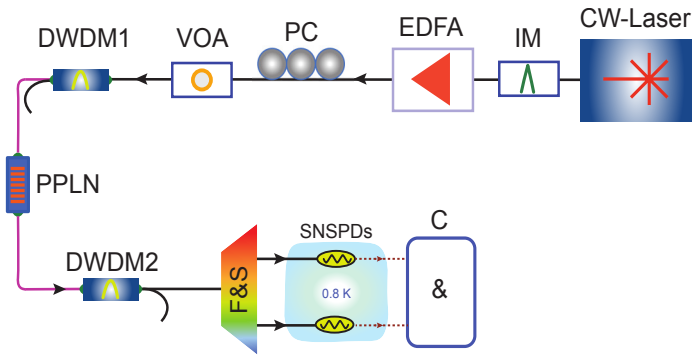

Fig. 1. Light from a CW 1532.7 nm laser goes through a polarization controller (PC) and an intensity modulator (IM) that can carve pulses. The light is then amplified in an erbium-doped fiber amplifier (EDFA). The intensity is controlled by an attenuator (VOA). The light is next sent through the waveguide (PPLN), and its output is collected by a dense wavelength division multiplexer (DWDM) filtering the leftover pump light out, and a series of filtering devices (F&S) which separate the different wavelengths involved in the processes. The leaked pump light is used for stabilizing interferometers. The detection is made by superconducting nanowire single photon detectors (SNSPD) kept at a temperature of 0.8 K in a cryostat, and the signals are analyzed using correlators (C).

The delta function in Equation 1 describes energy conservation, $f(\omega_p, \omega_s, \omega_i)$ is the phase matching (which depends on parameters such as crystal temperature and the periodic poling period [18]), and Equation 2 expresses that signal and idler photons must be created simultaneously within the coherence time of the pump. (The latter is for simplicity assumed to be infinity, according to the assumption of a monochromatic pump.) After splitting at a DWDM, the photons are detected using SNSPDs, and coincidence detections are counted using an electronic AND-gate with a coincidence window of 500 ps.

The quality of the source can be studied by looking at the cross-correlation coefficient $g^{(2)}_{s,i}$ (see Figure 2). This coefficient can be expressed by the number of coincidence detections C_c, the numbers of single detections C_s of the signal and C_i of the idler photons, and the coincidence detection window $\Delta\tau$ of 500 ps:

$$g^{(2)}_{s,i} = \frac{P_{s,i}}{P_s P_i} = \frac{C_c}{C_s C_i \Delta\tau}. \tag{3}$$

Here $P_{s,i}$, P_s, P_i are the probabilities for coincidence and single detections of the signal and idler photons, respectively. As is shown in Figure 2 a), selecting a lower pump power leads to a larger $g^{(2)}_{s,i}$, which implicates stronger quantum correlations. The weakening of quantum correlations at higher pump powers is related to the fact that SPDC is a probabilistic process. Hence, there is a probability that multiple photon pairs are generated, and this probability depends quadratically on the power of the 766.3 nm light created by the SHG process, meaning it is proportional to μ^2, where μ is the mean photon pair number for a 500 ps interval. This property is reflected in $g^{(2)}_{s,i}$ since P_s , P_i and $P_{s,i}$ are each, to first order, proportional to μ, and thus from Equation 3, $g^{(2)}_{s,i} \propto \mu/\mu^2 = 1/\mu$, indicating that it follows the ratio of single to double pairs. Furthermore, the source is considered to be quantum if $g^{(2)}_{s,i}$ is greater than 2 [19].

Figure 2 b) also shows that the single count rates follow a quadratic behavior with regard to the 1532.7 nm pump power. This is due to the cascaded SHG and SPDC processes: while SPDC

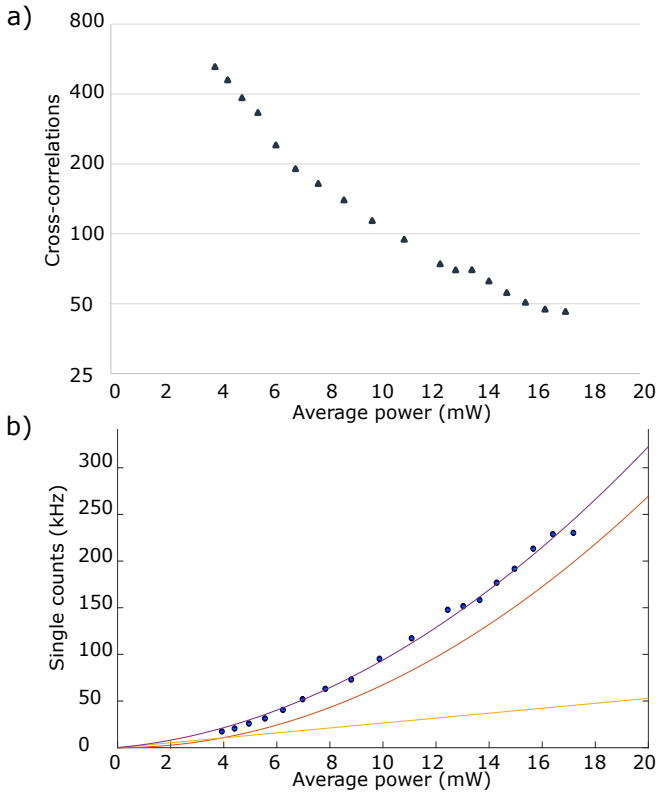

Fig. 2. **a**) Power dependence of the cross-correlation coefficient $g^{(2)}_{s,i}$ for the quasi-continuous-wave case. The $g^{(2)}_{s,i}$ is greater than two for the range of powers employed. **b**) Single counts vs average pump power for the quasi-continuous-wave case. The data (purple dots) is fitted to a second degree polynomial (purple line) so as to capture the noise and the photon pair generation contributions. At low power, the linear Raman noise (contribution represented by yellow line) is the main contribution, whereas at high powers it becomes negligible with respect to photon pair generation (orange line). The average power has to be optimized for a good $g^{(2)}_{s,i}$ and for high rates of coincidence detections.

increases linearly with the SHG power, the SHG itself scales quadratically with the pump power. Joining both in the same waveguide means that photon pair generation behaves quadratically with the power of the 1532.7 nm pump. Given the low mean photon pair number, $\mu \approx 0.01$, the multi-pair contribution is negligible compared to the single pairs. However, we also observe a linear component to the count rates, due to various sources of noise such as leaked pump light through the filters caused by a finite extinction ratio, and Raman noise inside the fibers bonded directly to the waveguide [20]. While the effect of leaked pump light can be diminished by cascading more filters, Raman noise is inevitable since it is spread over a broad frequency spectrum, including the filter passbands and thus the quantum channels [21].

2.1. Characterization of Raman scattering

Raman scattering is a process occurring when light interacts with phonons in materials such as the glass in optical fibers. This noise was identified as scattering for other cascaded sources, specifically Raman scattering in the experiments by Hunault [12] and Arahira [13] for their

non-degenerate photon pair sources, and Brillouin scattering by Hirosawa [11] for their degenerate source. The Raman scattering present in our source is shown in Figure 3 to increase linearly with respect to both the pump power and the length of fiber between the pump laser and the filters. The waveguide itself does not contribute much to the Raman noise: crystalline structures limit the energy of the phonons involved, and, as such, emission at the quantum channel wavelengths of 1530.3 nm and 1535.0 nm is minimal.

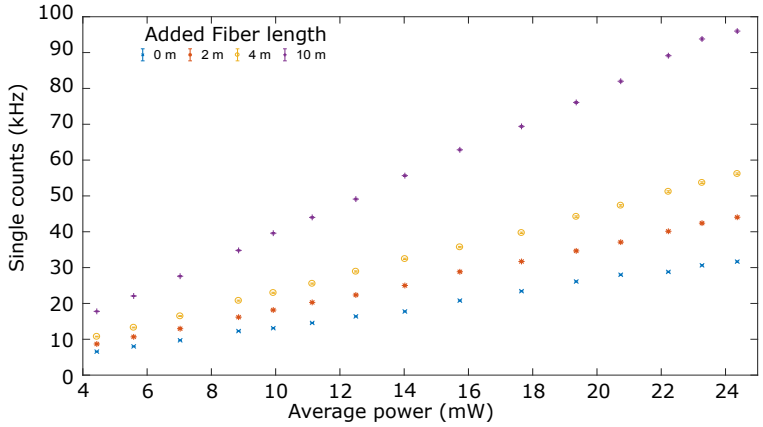

Fig. 3. Power dependence of the noise in the setup. The waveguide is replaced by an attenuator with the same loss as the waveguide, and a fiber of varying length. The figure shows the amount of extra fiber added to the setup, with the 0 m points representing the noise baseline. The main contribution to the noise is Raman scattering, which increases linearly with both the power and the length of fiber used. From the slope of the linear dependences at different lengths, an average Raman coefficient of 7.2×10^{-11} (km $\cdot$ nm)$^{-1}$ $\pm$ 0.2×10^{-11} (km $\cdot$ nm)$^{-1}$ is extracted. This is compatible with the typical values found in the literature that are of the order of 10^{-10} (km $\cdot$ nm)$^{-1}$.

The difference in pump power dependence between Raman noise and photon pair generation can be used to improve the signal-to-noise ratio. By increasing the pump power, the linear contribution of Raman noise can be made small in comparison with the quadratic photon pair generation. It therefore becomes advantageous to use quasi-continuous-wave pulses as opposed to CW to make full use of the high peak powers created by the EDFAs. This is the rationale for using pump pulses with a duration of 100 ns and a duty cycle of 5%. At high pump power, the photon pair generation can be made orders of magnitude larger than the Raman contribution, as shown in Figure 2. On the other hand, higher pump powers increase multi-pair emissions in SPDC, making the source less suitable for quantum information applications. The pump power thus needs to be optimized to diminish the relative effect of Raman noise while keeping a sufficiently large $g^{(2)}_{s,i}$. Indeed, the optimal method to limit Raman noise is to minimize the length of fiber before pump light is filtered, as illustrated by the reduced slopes for shorter fiber lengths in Figure 3. For the remaining investigations, we chose the shortest possible fiber length and a pump power of about 12 mW.

3. Results

To estimate the quality of energy-time entanglement generated from the source, the emitted pairs are subjected to two-photon interference using one or two interferometers. For such interference to occur, the bandwidth of the pump must be much smaller than the bandwidth of the created photons. In other words, the coherence time of the pump must be longer than the duration of the photons. Furthermore, the travel-time difference introduced by each interferometer, in our

case 1.4 ns, must be larger than the duration of each photon as well as the detector timing jitter, and smaller than the coherence time of the pump. These conditions are well satisfied in our setup. In particular, the coherent pump pulse of 100 ns duration acts like continuous-wave, i.e. narrowband light.

3.1. Two-photon interference – single interferometer

To establish a reference for the quality of entanglement, the photon pairs are sent to a single interferometer, as shown in Figure 4 a). We use a part of the rejected pump light from the DWDMs to adjust and stabilize its phase. Note that the filtered-out pump light is attenuated by 60 dB and therefore does not contribute in any noticeable way to the Raman noise in the experiment. The propagation of the state in Equation 2 through the interferometer leads to

$$\begin{aligned} |\psi\rangle' \quad &= \int dt \;\; |t+e\rangle_s \, |t+e\rangle_i + e^{i\phi} \, |t+e\rangle_s \, |t+l\rangle_i \\ &+ e^{i\phi} \, |t+l\rangle_s \, |t+e\rangle_i + e^{i(2\phi)} \, |t+l\rangle_s \, |t+l\rangle_i \, . \end{aligned} \tag{4}$$

with e (l) indicating that a photon took the short (or long) arm of the interferometer, and where ϕ is the phase gained in the long path of the interferometer. Restricting the coincidence measurement to the two indistinguishable–and hence interfering–terms (both photons travel through the same arm and are detected without time delay), the (post-selected) state of the photon pair becomes:

$$|\psi\rangle' = |e\rangle_s \, |e\rangle_i + e^{i(2\phi)} \, |l\rangle_s \, |l\rangle_i \, . \tag{5}$$

By scanning the phase of the interferometer, the expected sinusoidal coincidence detection rate is observed. Results are shown in Figure 4 b) with a visibility of $93.9\% \pm 0.4\%$. This demonstrates the suitability of our source for quantum communication applications. The pump power was selected such that the mean photon number was $\mu \approx 0.015$ per detection window of 500 ps. This type of interference has previously been used to generate frequency-bin entanglement exploiting the energy-time correlations of the photon pairs [22].

3.2. Franson interference – two interferometers

The high visibility obtained through two-photon interference is a strong indicator of the feasibility of more realistic and application-prone configurations such as Franson interference [23], which is required for Bell tests and quantum key distribution. In Franson interference, individual photons from an entangled pair interfere in two separate measurement devices, as illustrated in Figure 5 a). This leads to a sinusoidally varying coincidence count rate, similar to the case of the single interferometer described above, but now depending on the phases of either interferometer. For this type of interference to occur, the following additional condition must be followed: the two interferometers have to be aligned, i.e. the discrepancy between the travel-time differences must be smaller than the coherence time of each photon. Propagating the state of each photon in Equation 2 through the interferometers leads to

$$\begin{aligned} |\psi\rangle'' \quad &= \int dt \;\; |t+e\rangle_s \, |t+e\rangle_i + e^{i\phi_2} \, |t+e\rangle_s \, |t+l\rangle_i \\ &+ e^{i\phi_1} \, |t+l\rangle_s \, |t+e\rangle_i + e^{i(\phi_1+\phi_2)} \, |t+l\rangle_s \, |t+l\rangle_i \, , \end{aligned} \tag{6}$$

where $\phi_{1,2}$ are interferometer phases. After post-selection (keeping as before only the terms where the two photons coincide in time), the state of interest becomes

$$|\psi\rangle'' = |e\rangle_s \, |e\rangle_i + e^{i(\phi_1+\phi_2)} \, |l\rangle_s \, |l\rangle_i \, . \tag{7}$$

Fixing the phase of one interferometer and changing the phase of the other leads to the results shown in Figure 5 b). A visibility of $90.5\% \pm 0.6\%$ is observed, which is beyond the minimal

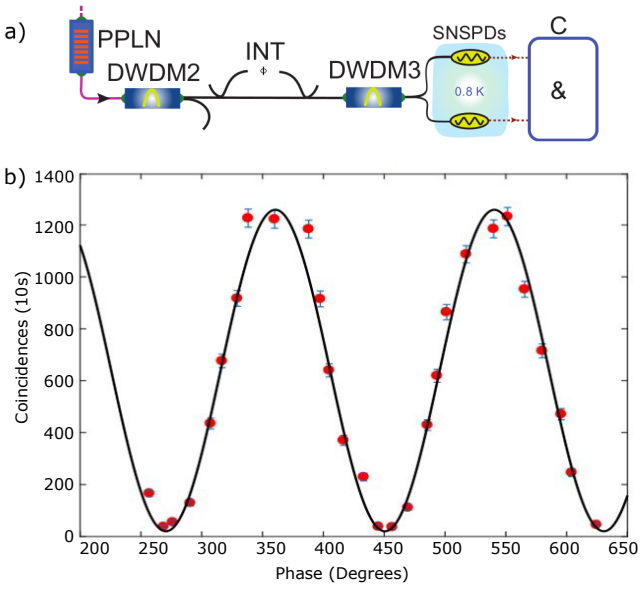

Fig. 4. **a**) Two-photon interference. The photon pairs are sent into a single interferometer with the two paths having a flight time difference of 1.4 ns and with active stabilization and control of the phase ϕ. The photons are then split in a DWDM and collected by SNSPDs. **b**) Measured two-photon interference with a visibility of 93.9% ± 0.4%.

values required for Bell tests as well as quantum key distribution, thereby indicating again the suitability of our source for applications in quantum communication. Note that the individual signal and idler counts remained constant during the scan as their coherence time (~ 20 ps, as determined by the filter bandwidth) is much smaller than the path length difference of 1.4 ns [24]. The pump power for these measurements was selected such that the mean photon number per detection window of 500 ps was $\mu \approx 0.011$.

4. Conclusion

A compact energy-time entangled photon pair source based on cascaded SHG and SPDC was presented. The main source of noise was identified as Raman scattering in the fibers connected to the waveguide – it is characterized by a Raman coefficient of $\left(7.2 \times 10^{-11} \pm 0.2 \times 10^{-11}\right)$ (km $\cdot$ nm)$^{-1}$. The quadratic behavior of photon pair generation was exploited to diminish the relative contribution of the linear Raman scattering while keeping the quantum nature of the source. Two-photon interference in a single as well as using two separate interferometers were then demonstrated, showing visibilities in excess of 90%, which suffices for applications in quantum communication. Taking the path-length difference of 1.4 ns in the interferometers and the width of the pump pulses of 100 ns into account, one can approximate the maximum theoretical visibility to be around 97.2%. The remaining Raman scattering can be further decreased by using integrated filters [25] such as coatings on the input and output waveguide surfaces that reject Raman photons and leaked light, respectively. The all-telecom nature of this source is

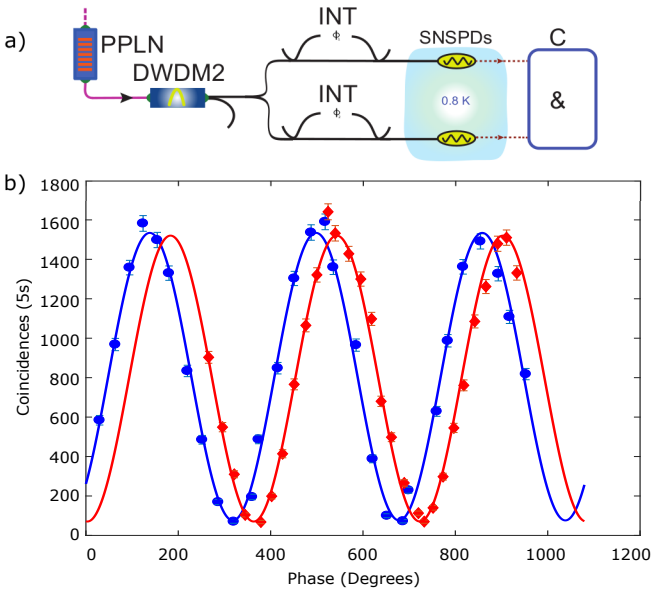

Fig. 5. **a**) Franson interference setup. The photon pairs are split in a DWDM, and each member is sent to an interferometer with two arms having a flight time difference of 1.4 ns, and with independent phase control $\phi_{1,2}$. The photons are then collected in the SNSPDs. **b**) Franson interference, where one interferometer is fixed while the other scans the phase. The two curves represent a phase difference of $\pi/4$ on the fixed interferometer. The visibility is computed from the fits as 90.5% ± 0.6%.

promising for quantum information applications, such as multipartite entanglement quantum networks [26], and its compactness might prove useful for applications with stringent restrictions, such as the limited space available on satellites [27].

Funding

This work was funded through Alberta Innovates Technology Futures (AITF) and the National Science and Engineering Research Council of Canada (NSERC). W.T. also acknowledges funding from the Netherlands Organization for Scientific Research (NWO) and as a Senior Fellow of the Canadian Institute for Advanced Research (CIFAR), and Q.Z. from the National Key R&D Program of China (2018YFA0307400) and the National Natural Science Foundation of China under grants 61775025 and 61405030.

Acknowledgments

The authors acknowledge V. Kiselyov for technical support. The detectors were provided by V.B. Verma and S.W. Nam.

Disclosures

The authors declare no conflicts of interest.

References

1. A. Einstein, B. Podolsky, and N. Rosen, "Can quantum-mechanical description of physical reality be considered complete?" Phys. Rev. **47**, 777 (1935).
2. J. S. Bell, "On the einstein podolsky rosen paradox," Phys. Physique Fizika **1**, 195–200 (1964).
3. B. Hensen, H. Bernien, A. E. Dreau, A. Reiserer, N. Kalb, M. S. Blok, J. Ruitenberg, R. F. L. Vermeulen, R. N. Schouten, C. Abellan, W. Amaya, V. Pruneri, M. W. Mitchell, M. Markham, D. J. Twitchen, D. Elkouss, S. Wehner, T. H. Taminiau, and R. Hanson, "Loophole-free bell inequality violation using electron spins separated by 1.3 kilometres," Nature **526**, 682–686 (2015). Letter.
4. W. Tittel, J. Brendel, H. Zbinden, and N. Gisin, "Quantum cryptography using entangled photons in energy-time bell states," Phys. Rev. Lett. **84**, 4737–4740 (2000).
5. N. Gisin, G. Ribordy, W. Tittel, and H. Zbinden, "Quantum cryptography," Rev. Mod. Phys. **74**, 145–195 (2002).
6. H.-K. Lo, X. Ma, and K. Chen, "Decoy state quantum key distribution," Phys. Rev. Lett. **94**, 230504 (2005).
7. E. Saglamyurek, M. Grimau Puigibert, Q. Zhou, L. Giner, F. Marsili, V. B. Verma, S. Woo Nam, L. Oesterling, D. Nippa, D. Oblak, and W. Tittel, "A multiplexed light-matter interface for fibre-based quantum networks," Nat. Commun. **7**, 11202 (2016). Article.
8. T. B. Pittman, B. C. Jacobs, and J. D. Franson, "Demonstration of feed-forward control for linear optics quantum computation," Phys. Rev. A **66**, 052305 (2002).
9. N. Sinclair, E. Saglamyurek, H. Mallahzadeh, J. A. Slater, M. George, R. Ricken, M. P. Hedges, D. Oblak, C. Simon, W. Sohler, and W. Tittel, "Spectral multiplexing for scalable quantum photonics using an atomic frequency comb quantum memory and feed-forward control," Phys. Rev. Lett. **113**, 053603 (2014).
10. R. C. Eckardt, H. Masuda, Y. X. Fan, and R. L. Byer, "Absolute and relative nonlinear optical coefficients of kdp, kd*p, bab/sub 2/o/sub 4/, liio/sub 3/, mgo:linbo/sub 3/, and ktp measured by phase-matched second-harmonic generation," IEEE J. Quantum Electron. **26**, 922–933 (1990).
11. K. Hirosawa, Y. Ito, H. Ushio, H. Nakagome, and F. Kannari, "Generation of squeezed vacuum pulses using cascaded second-order optical nonlinearity of periodically poled lithium niobate in a sagnac interferometer," Phys. Rev. A **80**, 043832 (2009).
12. M. Hunault, H. Takesue, O. Tadanaga, Y. Nishida, and M. Asobe, "Generation of time-bin entangled photon pairs by cascaded second-order nonlinearity in a single periodically poled $LiNbO_3$ waveguide," Opt. Lett. **35**, 1239–1241 (2010).
13. S. Arahira, N. Namekata, T. Kishimoto, H. Yaegashi, and S. Inoue, "Generation of polarization entangled photon pairs at telecommunication wavelength using cascaded $\chi(2)$ processes in a periodically poled $LiNbO_3$ ridge waveguide," Opt. Express **19**, 16032–16043 (2011).
14. J. Jin, M. Grimau Puigibert, L. Giner, J. A. Slater, M. R. E. Lamont, V. B. Verma, M. D. Shaw, F. Marsili, S. W. Nam, D. Oblak, and W. Tittel, "Entanglement swapping with quantum-memory-compatible photons," Phys. Rev. A **92**, 012329 (2015).
15. C. M. Natarajan, M. G. Tanner, and R. H. Hadfield, "Superconducting nanowire single-photon detectors: physics and applications," Supercond. Sci. Technol. **25**, 063001 (2012).
16. J. L. Jackel, C. E. Rice, and J. J. Veselka, "Proton exchange for high-index waveguides in $LiNbO_3$," Appl. Phys. Lett. **41**, 607–608 (1982).
17. Y. N. Korkishko, V. A. Fedorov, T. M. Morozova, F. Caccavale, F. Gonella, and F. Segato, "Reverse proton exchange for buried waveguides in $LiNbO_3$," J. Opt. Soc. Am. A **15**, 1838–1842 (1998).
18. D. S. Hum and M. M. Fejer, "Quasi-phasematching," Comptes Rendus Physique **8**, 180 – 198 (2007). Recent advances in crystal optics.
19. P. Sekatski, N. Sangouard, F. Bussières, C. Clausen, N. Gisin, and H. Zbinden, "Detector imperfections in photon-pair source characterization," J. Phys. B: At. Mol. Opt. Phys. **45**, 124016 (2012).
20. W. Zhang, Q. Zhou, J. R. Cheng, Y.-D. Huang, and J. D. Peng, "Impact of fiber birefringence on correlated photon pair generation in highly nonlinear microstructure fibers," The Eur. Phys. J. D-Atomic, Mol. Opt. Plasma Phys. **59**, 309–316 (2010).
21. Y. R. Shen and N. Bloembergen, "Theory of stimulated brillouin and raman scattering," Phys. Rev. **137**, A1787–A1805 (1965).
22. Q. Zhou, S. Dong, W. Zhang, L. You, Y. He, W. Zhang, Y. Huang, and J. Peng, "Frequency-entanglement preparation based on the coherent manipulation of frequency nondegenerate energy-time entangled state," J. Opt. Soc. Am. B **31**, 1801–1806 (2014).
23. J. D. Franson, "Bell inequality for position and time," Phys. Rev. Lett. **62**, 2205–2208 (1989).
24. M. Halder, A. Beveratos, N. Gisin, V. Scarani, C. Simon, and H. Zbinden, "Entangling independent photons by time measurement," Nat. Phys. **3**, 692–695 (2007).
25. D. Oser, S. Tanzilli, F. Mazeas, C. Alonso-Ramos, X. Le Roux, G. Sauder, X. Hua, O. Alibart, L. Vivien, É. Cassan, and L. Labonté, "High-quality photonic entanglement out of a stand-alone silicon chip," npj Quantum Inf. **6**, 31 (2020).
26. C. Monroe, R. Raussendorf, A. Ruthven, K. R. Brown, P. Maunz, L.-M. Duan, and J. Kim, "Large-scale modular quantum-computer architecture with atomic memory and photonic interconnects," Phys. Rev. A **89**, 022317 (2014).
27. M. Aspelmeyer, T. Jennewein, M. Pfennigbauer, W. R. Leeb, and A. Zeilinger, "Long-distance quantum communication with entangled photons using satellites," IEEE J. Sel. Top. Quantum Electron. **9**, 1541–1551 (2003).